

https://doi.org/10.1070/QEL16628

Laser-electron generators: the sources of narrow-band X-ray radiation for low-invasive coronary angiography

A.V. Vinogradov, N.V. D'yachkov, A.V. Polunina, N.L. Popov, V.I. Shvedunov

Abstract. **It is shown that the replacement of X-ray tubes used in coronary angiography with laser-electron X-ray generators improves the quality of imaging and (or) reduces the radiation load on the patient and the expenditure of the contrast agent. The main stages of the angiography procedure are implied to stay unchanged, and the advantages will be achieved at the expense of tuning the radiation spectrum to the absorption maximum of the contrast agent. The parameters of electron bunches and laser pulses interacting with them are determined that, on the one hand, provide the required flux of X-ray radiation and, on the other hand, obey the limitations imposed by the thermal and photoemission properties of the photocathode. These parameters can be implemented using the up-to-date achievements in laser and accelerator technology.**

Keywords: *coronary angiography, narrow-band X-ray radiation sources, laser-electron generators.*

1. Introduction

Low-invasive (interventional) coronary angiography (CAG) is a method of visualising the heart coronary vessels using X-ray radiation with catheterisation and injection of a contrast agent (based on iodine compounds) near the expected lesions of coronary arteries. During recent decades, it remains a golden standard of diagnostics for myocardial ischemia and other cardiac diseases [1–5]. In modern angiographs that allow the cardiac vessel condition to be observed in dynamics with the temporal resolution 0.01 s and the spatial resolution 0.15–0.2 mm, the sources of radiation are X-ray tubes [1]. In the present paper, following Ref. [6], we consider the possibility of replacing the X-ray tube used in coronarography with more perfect Thomson laser-electron X-ray source (LEXS), developed within the projects [7–12], etc. As shown by preliminary estimates [6], due to the narrow-band radiation of LEXS this replacement will reduce the radiation load for the patient, keeping the same or improving the quality of the angiographic images. Besides that, it may be possible to increase the spatial resolution and to decrease the concentration of iodine, which reduces the risk of allergic reaction in patients and makes the procedure cheaper. The advantages of LEXS over the X-ray tube are due to relatively small width of the radiation spectrum (Fig. 1) and the possibility of tuning the frequency near the iodine photoabsorption edge in order to optimise the above diagnostic parameters (see below).

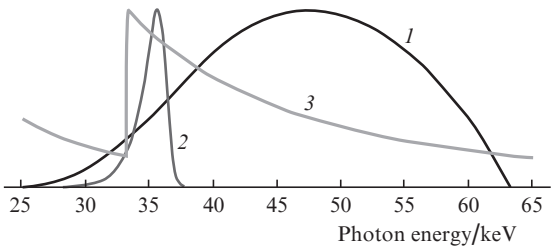

Figure 1. Spectra of the X-ray tube used in angiography (*1*) and the proposed LEXS (*2*) against the background of iodine absorption spectrum (*3*).

The studies of CAG with the X-ray tube replaced with a monochromated beam of synchrotron radiation [13–16] were carried out in the USA, Europe, the USSR, and Japan in 1986–2003 [17, 18]. The goal of the studies was to increase the safety of the procedure by eliminating the catheterisation and reducing the dose of the contrast agent injected intravenously, as well as by subtracting the images, obtained at different sides of the K-edge in the iodine photoabsorption spectrum. In this case, the main advantages of synchrotron radiation (the collimation and the possibility of frequency tuning of the beam) were used. The developed technique was tested in hundreds of patients; however, it is still not used in clinical practice. The number of publications on this issue has significantly reduced from 2003.

In contrast to Refs [13–18], in the present paper, as in Ref. [6], we do not give up the catheterisation and only replace the radiation source. It is assumed that it will be possible to save the rest stages of the angiographic procedure (contrasting, multi-projection recording, fluoroscopy, dynamical fixation of images on a hard disc, etc. [2–4]). The main purpose of replacing the X-ray tube with LEXS is the improvement of the informativity and safety standards of the procedure: the reduction of radiation and contrast agent doses, received by

A.V. Vinogradov, N.L. Popov P.N. Lebedev Physical Institute, Russian Academy of Sciences, Leninsky prosp. 53, 119991 Moscow, Russia;
N.V. D'yachkov P.N. Lebedev Physical Institute, Russian Academy of Sciences, Leninsky prosp. 53, 119991 Moscow, Russia; Moscow Institute of Physics and Technology (State University), Institutskii per. 9, 141700 Dolgoprudnyi, Moscow region, Russia;
e-mail: dyachkov@sci.lebedev.ru;
A.V. Polunina City Clinical Hospital No. 17, ul. Volynskaya 7, 119620 Moscow, Russia;
V.I. Shvedunov P.N. Lebedev Physical Institute, Russian Academy of Sciences, Leninsky prosp. 53, 119991 Moscow, Russia;
D.V. Skobeltsyn Institute of Nuclear Physics, M.V. Lomonosov Moscow State University, Vorob'evy gory, 119234 Moscow, Russia

Received 6 February 2018; revision received 27 April 2018
Kvantovaya Elektronika **48** (6) 565–572 (2018)
Translated by V.L. Derbov

the patient, as well as the improvement of spatial and temporal resolution at the expense of more suitable physical properties of the new radiation source.

2. Main parameters of CAG: radiation dose, image quality, iodine concentration, spatial resolution. Choosing the optimal energy of the quantum from a narrow-band source

X-ray images used in CAG for the diagnostics of contrasted vessels are obtained with an exposure of the order of a millisecond or a few milliseconds and a repetition rate up to 30 frames per second. This imposes sufficiently rigid requirements on the radiation intensity of the source. X-ray tubes of angiographs operate at voltages 60–120 kV (in Fig. 1 the spectrum of a tube operating at the anode voltage 63 kV is shown), so that the mean energy of the X-ray quantum may exceed the energy corresponding to the photoabsorption edge of the contrast medium (iodine) by 1.5 times and more. Obviously, in the case of the maximum of the source radiation spectrum coincident with the wavelength of the K-edge of iodine the efficiency of using the contrast agent would increase. However, it requires the reduction of the tube anode voltage, which would lead to unacceptable fall of the X-ray radiation intensity. It is impossible to compensate it by increasing the current because of anode degradation and cathode limitations [19].

In other words, the high intensity of the source needed to obtain the CAG images together with the limitations determined by the physical properties of the cathode and anode materials do not allow satisfactory matching of the source spectrum with the absorption spectrum of iodine in the case of an X-ray tube. Note that the spectrum of radiation emitted by the X-ray tube anode is much broader than the peak of iodine photoabsorption, so that a narrow-band tunable source would be preferable, provided that its intensity is sufficient for video recording, prescribed by the above CAG protocols (1–2 ms, 30 Hz). How the use of such a source will affect the main medical characteristics of CAG? To answer this question, let us consider the expression for the radiation dose $D(E)$ required to obtain a single angiographic image with a narrow-band source [6]

$$D(E) = \frac{M^2(\mathrm{CNR})^2}{m} E(\exp(\mu L) - 1) \times \frac{1 + \exp[-(\kappa - \mu)\delta]}{\{1 - \exp[-(\kappa - \mu)\delta]\}^2}, \quad (1)$$

where E is the photon energy; M^2 is the number of angiographic image pixels; CNR is the contrast ratio; m and L are the mass and the thickness of the patient's body; κ and μ are the absorption coefficients of the contrast agent in the coronary vessel and in the surrounding medium, depending on the quantum energy; and δ is the vessel diameter.

In accordance with Eqn (1), Fig. 2 presents the dependences of the basic CAG parameters on the photon energy. From the presented results, it follows that the replacement of the X-ray tube with a tunable narrow-band source allows one to improve the CAG parameters by optimising the X-ray quantum energy. In particular, the radiation dose can be reduced by several times [20] keeping the same level of image quality. For the optimal quantum energy 38 keV, the value of the dose $D(E)$ per frame for the image quality CNR = 15 amounts to 20 μSv, which corresponds to $N = 2 \times 10^{11}$ photons (Fig. 2a). These values determined within the accuracy of 15%–20% agree with those obtained in Ref. [6] using a semiempirical method, namely, 23 μSv, $N = 2{,}5 \times 10^{11}$, the optimal energy being 43 keV. The semiempirical method [6] is based on using the data of the automatic dose rate control systems of a commercial Allura FD10 angio-

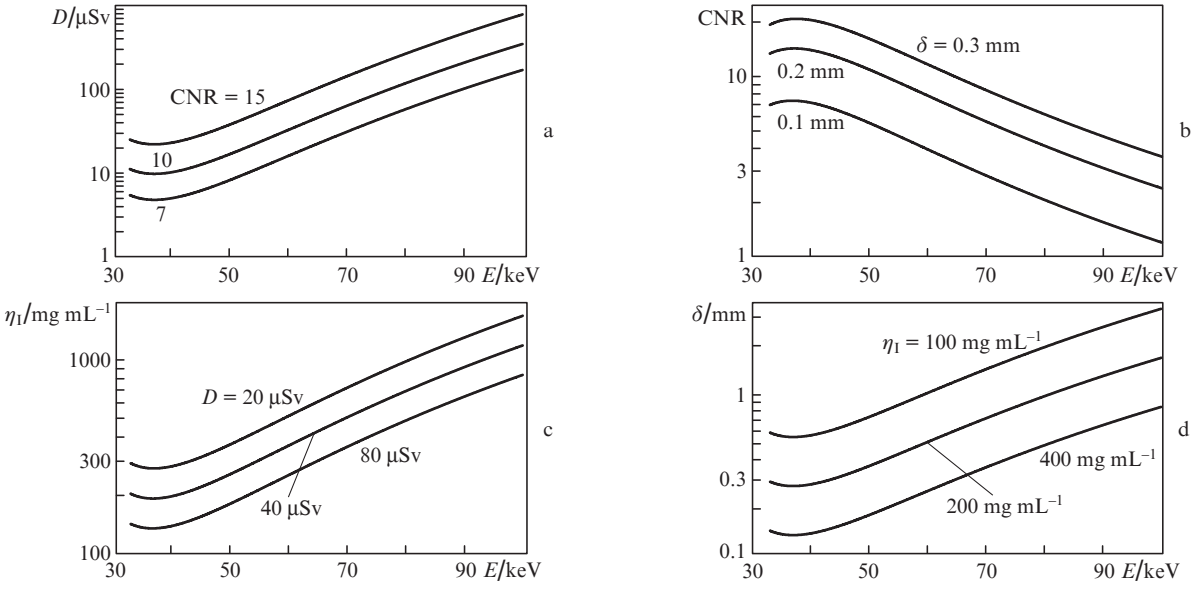

Figure 2. Medical CAG parameters [see Eqn (1)]. Dependence of (a) the radiation dose D received by the patient, (b) the contrast of images CNR, (c) the iodine concentration η_I in the contrasting solution, and (d) the spatial resolution δ of the monochromatic CAG on the energy of the X-ray radiation quantum E. The default values of the parameters not indicated in the corresponding plots are $\delta = 0.2$ mm, $D = 20$ μSv, $\eta_I = 400$ mg mL^{-1}, CNR = 15, $M = 256$. The calculations were performed for the mass of the patient $m = 75$ kg and the thickness of his body $L = 20$ cm.

graphic complex [19], and Eqn (1) is used only as a model dependence of the dose on the photon energy. Thus, here the properties of the existing radiation detectors are effectively taken into account. Hence, for further estimation of the parameters of lasers and electron accelerator used in LEXS for CAG we assume the energy of the photon $E = 40$ keV and the number of photons per frame $N = 3 \times 10^{11}$, preserving the existing standards of exposure time (1–2 ms) and spatial resolution (0.15–0.2 mm) [1, 19].

The diagnostics of vessel functioning is performed in two CAG regimes, fluoroscopy and video recording. In the latter case, the radiation dose per frame is higher by about an order of magnitude [2–4]. The total number of frames is about a thousand; the repetition rate does not exceed 30 frames per second. The above protocols and parameters of the modern CAG are based on the quantitative studies of the radiation dose in different regimes with simultaneous recording of a large number of medical and technical parameters. Such studies are carried out in many countries within the national health care programmes using commercial angiographs. The obtained results differ within an order of magnitude and depend on the equipment type, age, weight and condition of patient, the physician experience, and many other factors [21–30].

As already mentioned, the main goal of our study is to improve these parameters and, therefore, the quality of diagnostics, by replacing the radiation source (X-ray tube) with LEXS. The principle of operation and properties of LEXS are described below.

3. General information on LEXS. Total yield of X-ray radiation from collision of a laser pulse with a bunch of electrons

The X-ray radiation from LEXS is a result of Thomson or Compton scattering of laser radiation by relativistic electrons in the beams of linear or cyclic accelerators. Among the first experimental works on the observation of the effect let us mention Ref. [31]. F. Carroll [32] proposed the idea of practical application of LEXS in medicine. At present, there are a number of operating setups for different applications [10, 33] and those under construction [11, 12, 34].

The main fundamental problem of constructing LEXS is related to the small value of the Thomson scattering cross section ($\sigma_T = 6.6 \times 10^{-25}$ cm^2). The solution of this problem requires not only increasing the fluxes in the interacting beams of electrons and photons, but also decreasing the transverse size of their interaction region. Since the interaction occurs in vacuum, this is possible only at the expense of tight focusing of radiation, in which both the transverse size of the focal region (waist) and its longitudinal size become small. For the maximal efficiency of the beams interaction, it is necessary to provide as many potential interaction events in the waist region as possible. One can achieve it by shaping both electron and photon fluxes as a sequence of pulses with the spatial length not exceeding the waist length. It is easy to estimate that for the transverse size of the interaction region of the optical pulse (in terms of Gaussian beams) $2\sigma_L = 10$ μm and the wavelength $\lambda_L \approx 1$ μm, the required pulse duration $\tau = 2Z_R/c$ (Z_R being the Rayleigh length) will amount to a few picoseconds. Quantitative estimates of these parameters will be presented below, and here we briefly describe the simplest LEXS scheme that allows the required yield of X-ray radiation.

Figure 3 presents the block diagram of LEXS based on a linear accelerator. The electron bunches of picosecond duration are emitted from the photocathode by the pulses of a special picosecond photocathode laser (PCL) operating in the mid-UV range. The requirements to the PCL depend on the choice of photocathode material. In the present paper, we restrict ourselves to considering the copper photocathode. Although its quantum efficiency is low ($\eta_c \sim 10^{-4}$), it has high heat conductivity that provides its higher resistance to radiation loads. To irradiate such photocathode, a suitable PCL is the one that uses the fourth harmonic of the neodymium laser (the photon energy $\hbar\omega_{cL} = 4.8$ eV).

The obtained bunches of electrons arrive at the acceleration unit, where they acquire the necessary energy of a few tens of MeV. The acceleration unit is a system of coupled microwave cavities, in which the up-to-date level of technology allows the achievement of the mean accelerating field above 25 MV m^{-1} without using superconducting elements [35]. Hence, the size of the required acceleration module (2–3 m) is, generally speaking, comparable with the overall dimensions of the rest units of LEXS.

Electron bunches accelerated by the above unit are focused into the region of interaction with the pulses of laser radiation, located inside the optical accumulator (power enhancement cavity or circulator). The use of the optical accumulator allows the mean effective power of laser pulses, interacting with the electron bunches, to be increased by 2–4 orders of magnitude as compared to the power of the pump laser at the expense of increasing their energy (in the case of a cavity) and repetition rate (in the case of a circulator). As a result of the interaction, a narrow X-ray beam (~10 mrad) is generated consisting of trains of picosecond pulses, which are directed onto the studied object.

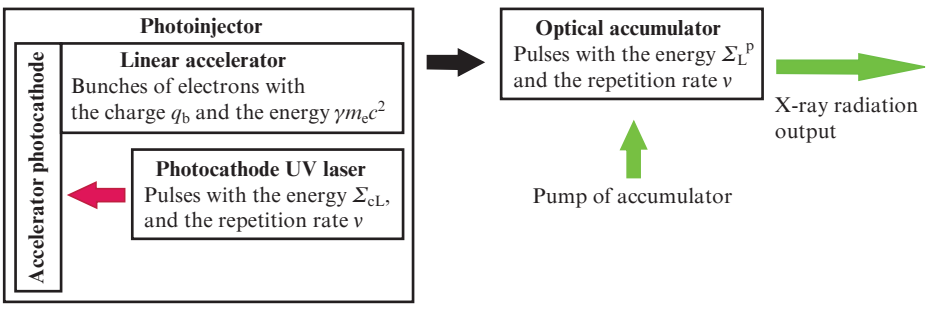

Figure 3. Block diagram of LEXS based on a linear accelerator.

Now let us present brief but rigorous derivation of the basic expressions, necessary to calculate the LEXS intensity based on the first principles.

The beam generated by LEXS consists of repeating X-ray flashes with the repetition rate ν that accompany the collisions of large number of photons ($N_L \sim 10^{17}$) and electrons ($N_e \sim 10^{10}$), which we consider here as classical relativistic particles with the concentrations $n_L(\boldsymbol{r},t)$ and $n_e(\boldsymbol{r},t)$. Using the definition of the effective cross section σ, the yield dN (the number of events, in our case the appearance of X-ray photons) from the element of volume $d\boldsymbol{r}$ during the time dt for any reaction in the system of coordinates, where one kind of particles (in our case electrons) is at rest, is

$$dN = \sigma' c n_e' n_L' d\boldsymbol{r}' dt'. \tag{2}$$

The primes denote the quantities in the coordinate frame attached to the electrons. The total number of events dN does not depend on the coordinate system. The other parameters in Eqn (2), except for the invariant differential cross section σ' defined in the coordinate system, where the electrons are at rest, are transformed under the transition to the laboratory frame, which yields

$$dN = \sigma'[c - (\boldsymbol{\kappa}_L, \boldsymbol{v})] n_e n_L d\boldsymbol{r}\, dt, \tag{3}$$

where $\boldsymbol{\kappa}_L$ is the unit vector for the photon direction of motion; and $\boldsymbol{v}$ is the velocity of the electron. It is easy to derive this formula from Eqn (2) keeping in mind that $d\boldsymbol{r}\, dt$ is a scalar, and $\{m\boldsymbol{v}, nc\}$ is a four-dimensional current vector [36, 37]. Expression (3) describes a wide scope of processes with the participation of photons. For many practical estimates the case of head-on collision is useful $[(\boldsymbol{\kappa}_L, \boldsymbol{v}) = -c]$, for which the calculations lead to relatively simple formulae [38].

Let us use Eqn (3) to determine the total number of photons in the Thomson scattering of the laser pulse by the relativistic electron bunch. In this case $\sigma' = \sigma_T$ is the total cross section of Thomson scattering. Integrating Eqn (3) over $d\boldsymbol{r}\, dt$ and keeping in mind that the X-ray radiation arising in the head-on collision is mainly directed forward along the direction of the electron motion, we obtain the total number of X-ray photons

$$N = 2c\sigma_T N_e N_L J, \tag{4}$$

where

$$J = \int_{-\infty}^{\infty} \iiint n_e(\boldsymbol{r},t)\, n_L(\boldsymbol{r},t)\, d\boldsymbol{r} dt.$$

Here, in contrast to Eqns (2) and (3), n_e and n_L denote the reduced values normalized to 1, rather than the concentrations of particles themselves. The integral J is determined exclusively by the geometry of the colliding pulses (bunches) and the degree of their coincidence in space and time. It is related neither to the interaction type, nor to the result of the collision. Consider the collision of two Gaussian pulses, in which the distribution of reduced concentrations in space and time has the form:

$$n_e(x,y,z,t) = \frac{\exp\left\{-\dfrac{x^2+y^2}{2\sigma_e^2[1+(z/\beta)^2]} - \dfrac{(z-ct)^2}{2l_e^2}\right\}}{(2\pi)^{3/2} l_e \sigma_e^2 [1+(z/\beta)^2]},$$

$$n_L(x,y,z,t) = \frac{\exp\left\{-\dfrac{x^2+y^2}{2\sigma_L^2[1+(z/Z_R)^2]} - \dfrac{(z+ct)^2}{2l_L^2}\right\}}{(2\pi)^{3/2} l_L \sigma_L^2 [1+(z/Z_R)^2]}. \tag{5}$$

Here, according to [39], σ_e and σ_L are the radii; β and Z_R are the longitudinal sizes of the waists of the electron and laser beam; and l_e and l_L are the lengths of the pulses at half-maximum level. Note that the radii and longitudinal sizes of the waists are related via the normalised emittance ε_n of the electrons and the wavelength λ_L of the laser radiation in the following way:

$$\beta = \frac{\gamma\sigma_e^2}{\varepsilon_n}, \quad Z_R = \frac{4\pi\sigma_L^2}{\lambda_L}, \tag{6}$$

where γ is the relativistic factor of the electrons.

Substituting Eqn (5) into Eqn (4) we obtain

$$J = \frac{g(y)}{4\pi c(\sigma_e^2 + \sigma_L^2)}, \tag{7}$$

where

$$g(y) = \sqrt{\pi y}\, e^y \operatorname{erfc}\sqrt{y};$$

$$y = \frac{2(\sigma_e^2+\sigma_L^2)}{l_e^2+l_L^2}\left(\frac{\sigma_e^2}{\beta^2} + \frac{\sigma_L^2}{Z_R^2}\right)^{-1} = 2\left(\frac{l_e^2+l_L^2}{\beta^2}\frac{\sigma_e^2}{\sigma_e^2+\sigma_L^2} + \frac{l_e^2+l_L^2}{Z_R^2}\frac{\sigma_L^2}{\sigma_e^2+\sigma_L^2}\right)^{-1}.$$

From Eqns (4) and (7) we finally obtain [38]

$$N = \frac{N_e N_L \sigma_T}{2\pi(\sigma_e^2+\sigma_L^2)} g(y), \quad g(y) = \begin{cases} 1, & y \gg 1, \\ \sqrt{\pi y}, & y \ll 1. \end{cases} \tag{8}$$

The dependence $g(y)$ is illustrated in Fig. 4. With Eqns (7) and (8) taken into account, from this dependence it follows that the maximal yield of X-ray radiation corresponds to $g(y) \approx 1$ and does not change essentially at $y > 1$. This criterion can be taken as a base for estimating the duration of the colliding pulses and bunches. If we assume that $\sigma_e = \sigma_L$ and $\varepsilon_n/\gamma \ll \lambda_L$, then the pulse duration is

$$\tau = 2\frac{l_L}{c} = 2\sqrt{2}\, Z_R = 8\sqrt{2}\frac{\pi}{c}\frac{\sigma_L^2}{\lambda_L}. \tag{9}$$

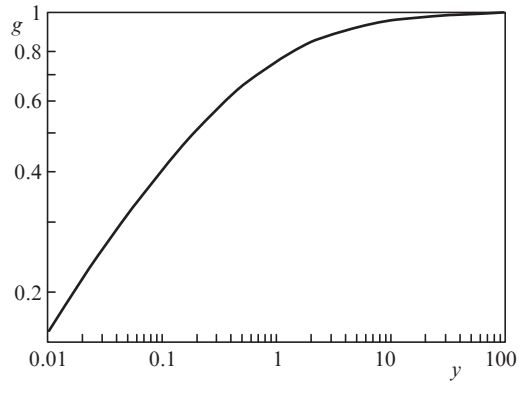

Figure 4. Dependence of g on y.

4. LEXS for CAG based on a linear accelerator

Now let us apply the derived expressions to LEXS used in CAG. The brief information about it is presented in Ref. [39]. Note that the relative spectrum width amounts to 10%–15% and the divergence $\gamma^{-1} \approx 10^{-2}$. This allows us to use the results of Section 2 and to assume that all X-ray photons, described by Eqn (8), hit the necessary area of the patient body and serve for diagnostics.

Since the radiation source for CAG must operate with the frame rate 30 Hz, the number of photons per frame (macro-pulse), N_p should be no smaller than 3×10^{11}, and the duration of the macro-pulse itself τ_p should be no greater than 1–2 ms, the required mean flux of photons during the above time is 3×10^{14} s^{-1}, and the mean flux during the recording is 9×10^{12} s^{-1}, i.e., the duty cycle amounts to 3%. Below, Eqn (8) is used to show that to achieve these values one should satisfy rather high requirements to the components of LEXS, corresponding to the current level of accelerator and laser technology [40–43]. In most cases, it is due to fundamental reasons, namely, the thermal, electric, optical, and other properties of materials. As already mentioned above, the reasons of such sort restrict the capabilities of modern angiographic systems, do not allow the matching of spectral maximum of the X-ray source with the absorption maximum of the contrast agent (iodine) and implementing the operation regimes most efficient for improving the image quality. At the same time, the radiation spectrum of LEXS is determined by the energy of electrons and laser quanta, and the difficulties related to its tuning are not so essential.

In the analysis of elements of the accelerator and laser modules of LEXS, including the sources of microwave energy, photocathodes, cavities, etc., we benefit from the capabilities of commercial technologies or the results confirmed experimentally. For the first time such consideration was performed ten years ago [44, 45] for a wide scope of photocathode materials and different types of LEXS. In the present paper, we consider the widely used copper cathode, and the main attention is paid to the specific requirements that follow from the CAG protocol for the photoinjectors and the lasers used in them, with the up-to-date level of their development taken into account.

Let us estimate the parameters of LEXS that can produce $N_p = 3 \times 10^{11}$ photons during the time $\tau_p < 1–2$ ms. To this end, let us return to Eqn (8) that determines the photon yield from one electron bunch, one macro-pulse containing $n_b = \nu\tau_p$ of them. Setting for simplicity $\sigma_L = \sigma_e$ and $g(y) \approx 1$, we obtain

$$N_p = n_b \frac{N_e N_L \sigma_T}{4\pi\sigma_e^2} = \frac{\gamma Q N_L \sigma_T}{4\pi e\beta\varepsilon_n} = N = \Gamma N_L \sigma_T, \qquad (10)$$

where

$$\Gamma = \frac{\gamma Q}{4\pi e\beta\varepsilon_n}.$$

Here N_e and $Q = n_b q_b$ is the total number of electrons and the total charge of the beam in one macro-pulse, containing n_b bunches of charge q_b. For the estimates in Eqn (7) in correspondence with the energy of the K-edge absorption jump of iodine we will use moderately small value of β (1 cm) and $\gamma = 90$. The problem is to optimise the acceleration unit with respect to the parameters entering the expression for Γ (the charge and the number of bunches q_b and n_b, the emittance ε_n that determines the size of the interaction region σ_e) in order to obtain the maximal yield of X-ray photons.

Since the electrons are knocked from the cathode by the PCL radiation, the heat resistance of the cathode material (copper) determines the values of the first two parameters. The simplest model used by us to estimate the maximal value of Q is shown in Fig. 5. We assume that all the PCL energy required to produce the necessary number of electrons is spent on heating the cathode region, over which the heat from the irradiated spot can spread during the time τ_p. The emittance, in turn, is mainly determined by the action of the spatial charge forces (for a large charge of bunches) or by thermal straggling of momentum of photoelectrons (for small charge). From the known Γ and exposure dose N_p, using Eqn (10), one can find the number of photons N_L in the laser pulse stored in the accumulator.

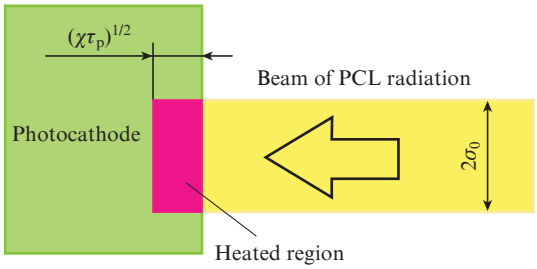

Figure 5. Model for estimating the photocathode heating near the PCL radiation spot. The PCL radiation energy required to produce the necessary number of electrons is fully absorbed at the irradiated surface with the radius σ_0 and is used to heat the region of heat propagation. The overheating criterion is the achievement of cathode material melting temperature in this region during the time τ_p.

First, let us consider bunches possessing the large charge $q_b \geqslant 100$ pC. In tis case the emittance ε_n is determined mainly by the effect of the spatial charge forces, and the ratio q_b/ε_n becomes a constant, so that increasing the charge beyond 100 pC has no sense [46]. For qualitative estimates of such charges, one can use the ratio $q_b/\varepsilon_n \approx 2.5 \times 10^{-4}$ C m^{-1} and the focusing spot radius at the photocathode $\sigma_0 = 0.8$ mm. The total charge Q is determined by the laser energy Σ_{cL}^p hitting the photocathode during a single macro-pulse (operation cycle) of the accelerator, which we assume to be nearly equal to the exposure time $\tau_p \approx 1$ ms. Then, in correspondence with the heat balance equation in the region having the depth $\sqrt{\chi\tau_p}$ (χ being the thermal diffusivity, see Fig. 5), adjacent to the focusing spot of the laser radiation with the radius σ_0, we have

$$\Sigma_{cL}^p = \pi\sigma_0^2 \sqrt{\chi\tau_p}\, C\rho\Delta T. \qquad (11)$$

Here C and ρ are the specific heat capacity and the density of the photocathode material, and $\Delta T = T - T_0$ is the photocathode heating during the time τ_p. For the copper photocathode, substituting the values $\chi = 1.2$ cm^2 s^{-1}, $C = 385$ J kg^{-1} deg^{-1}, $\rho = 8.9$ g cm^{-3}, $\Delta T \approx 1000$ K, and $\tau_p \approx 1$ ms into Eqn (11), we obtain the total energy of the photocathode laser macro-pulsea $\Sigma_{cL}^p = 2.4$ J. For the quantum efficiency $\eta_c = 10^{-4}$ (in Ref. [47] 1.3×10^{-4}) and the laser photon energy $\hbar\omega_{cL} = 4.8$ eV, this corresponds to the charge $Q = n_b q_b = 50$ μC and the number of bunches $n_b = 5 \times 10^5$. Assuming the repetition rate of bunches ν to coincide with the repetition rate of laser

Table 1. Parameters of the accelerator and laser units of LEXS for CAG.

Parameters	Values of the parameters		
	1	2	3
Charge of a single EB q_b/pC	100	15	100
PCL pulse energy Σ_{cL}/μJ	5	0.75	5
EB emittance ε_n/m	4×10^{-7}	10^{-7}	4×10^{-7}
PCL quantum energy $\hbar\omega_{cL}$/eV	4.8	4.8	4.8
PCL beam spot radius at the PC σ_0/mm	0.8	0.2	0.8
Quantum efficiency of PC η_c	10^{-4}	10^{-4}	10^{-4}
EB relativistic factor γ	90	90	90
EB beta function in the IR β/cm	1	1	1
Gaussian IR diameter σ_e/μm	6.6	3.3	6.6
PCL energy per frame Σ^p_{cL}/J	2.4	0.15	2.4η
Total charge of EB per frame Q/μC	50	3.1	50η
MP of the EB flux per frame P_e/MW	2.5	0.15	2.5η
Total EB number per frame n_b	5×10^5	2×10^5	$5\eta \times 10^5$
EB repetition rate ν/MHz	500	200	500η
MP of PCL per frame P^p_{cL}/W	2400	150	400.5η
MP of PCL per second P_{cL}/W	72	4.5	72η
Coefficient Γ from Eqn (7)/cm^{-2}	5.6×10^{19}	1.4×10^{19}	$5.6\eta \times 10^{19}$
Energy of a single LP Σ^p_L/mJ)	1.5	6.1	$1.5\eta^{-1}$
MP of LP per frame P^p_L/MW	0.75	1.2	0.75
MP of LP per second P_L/kW	25	40	25
LP wavelength λ_L/nm	1060	1060	1060
LP and EB duration τ/ps	4.9	1.2	4.9

Note. The values of parameters in columns 1 and 2 correspond to the maximal load of photocathode (heating by $\Delta T \approx 1000$ K during one macro-pulse), the values in column 3 imply the optimisation of the parameters of column 1 at the expense of reducing the pulse repetition rate by η times. For all cases the duration of one macro-pulse (frame) is $\tau_p = 1$ ms and the repetition rate of frames is 30 Hz; (EB) electron bunch; (PCL) photocathode laser; (PC) photocathode; (IR) interaction region of electron with laser radiation in the accumulator; (MP) mean power; (LP) – laser pulse, formed in the optical accumulator.

pulses in the accumulator and photoinjector, one can easily find the pulse (averaged over a macro-pulse) and the mean (for the recording rate 30 s^{-1}) power of the PCL and the laser radiation in the accumulator of photons. All these quantities are presented in the first column of Table 1.

To choose the most convenient regime of the accelerator unit operation, let us consider small charges of electron bunches $q_b \leqslant 15$ pC. In this case, the value of ε_n is mainly determined by such factors as the time dependence of the accelerating field, the magnitude of the magnetic field at the cathode, the thermal emittance, and after the appropriate optimisation of the microwave gun it approaches the value of the thermal emittance [46]. As a practical limit, one can consider $\varepsilon_n \approx 10^{-7}$ m for the radius of the spot on the photocathode $\sigma_0 = 0.2$ mm. The corresponding parameters of the acceleration and laser module are presented in the second column of Table 1.

In the present paper, we restrict ourselves to considering LEXS based on linear accelerators with copper photocathode and accumulators of laser radiation. In this case, as seen from Table 1, the large charge of the bunches gives rise to excess requirements imposed on the photocathode laser and the pulse power of the beam. The requirements to the accumulator of photons in this case correspond to the results of Ref. [48] (the energy $\Sigma^p_L = 2.7$ mJ, the power $P^p_L = P_L = 0.76$ MW). In turn, the injector with a copper photocathode and a linear accelerator for LEXS with the small charge of bunches ($q_b \leqslant$ 15 pC), on the contrary, possess a low pulse power of the beam. However, the photon accumulator in column 2 of Table 1 excels the highest figures demonstrated to date both in energy and in power [48]. A more acceptable version from all points of view can be chosen using the parameters of column 3. Here the case of a large bunch charge is presented with the scaling factor η taken into account. In particular, for $\eta = 0.2$ the total charge Q and other parameters of the electron beam decrease by five times, which essentially softens the requirements to the accelerator and leads to more realistic characteristics of the photocathode laser (see Ref. [49]). In this case, the required energy of the pulse stored in the accumulator exceeds the result of Ref. [48] almost by three times. At the same time, the pulse power P^p_L corresponds to the achieved one, and the required mean power P_L appears to be smaller by 30 times.

5. Discussion and conclusions

The proposed new method of CAG imaging consists in the replacement of the X-ray tube with the narrow-band source. In contrast to a number of other methods [13–16, 50–54] its aim and advantage is not to reject catheterisation, but to reduce the radiation dose together with the possibility of improving the quality of images and decreasing the contrast agent expense. It is expected that the rest technologies of the interventional CAG (recording and processing of images, sur-

vey protocols, etc.) will stay unchanged, which significantly simplifies the practical implementation of the method.

The laser-electron generator, the development of which starting from Ref. [32] has been carried out in many research centres, can be such a narrow-band X-ray source. However, the already operating LEXS and those being designed still do not satisfy the requirements of present-day CAG by both the mean power and the pulse one. The version considered in the present paper is based on linear accelerators and looks implementable based on the up-to-date laser and accelerator technologies. It is possible that the system comprising a storage ring will appear to be more energy saving although less compact. In the further analysis one should consider in more detail the laser module, particularly, the photon accumulator with the alternative of resonator [48, 55] versus circulator [56, 57] taken into account. The present paper formulates only the requirements to the stored laser energy $\Sigma_{\mathrm{L}}^{\mathrm{p}}$.

In conclusion, we note that the replacement of the X-ray tube with the narrow-band X-ray source can essentially reduce the radiation load for the patient and optimise other parameters of the cardiac vessels diagnostics, including the image quality, spatial resolution, concentration and expense of contrast agents.

The laser-electron generator based on a linear accelerator and photon accumulator possesses the mean and pulse power required for CAG. Its basic components, apparently, can be created basing on the existing laser and accelerator technologies.

The analysis of the thermal regime of the photocathode and the dynamic properties of the generated electron beam allowed the formulation of the requirements to the photoinjector laser and photon accumulator.

The applied calculation technique can be useful for the development of other LEXS applications, not rarely related to the requirements to the X-ray beam that are rather hard to satisfy [58–61].

Acknowledgements. The authors are grateful to M.V. Gorbunkov for thorough discussions of the work and to I.A. Artyukhov, A.E. Drakin, and R.M. Feshchenko for reading the manuscript.

The work was supported by the Presidium of the Russian Academy of Sciences (Programme 'Urgent Problems of Photonics, Probing of Inhomogeneous Media and Materials').

References

1. Stefanini G.G., Windecker S. *Circulation*, **131** (4), 418 (2015).
2. Moscucci M. *Grossman & Baim's Cardiac Catheterization, Angiography, and Intervention* (USA, Philadelphia: LWW, 2013).
3. Savchenko A.P., Cherkavskaya O.V., Rudenko B.A., Bolotov P.A. *Internentsionnaya kardiologiya. Koronarnaya angiografiya i stentirovaniye* (Interventional Cardiology. Coronary Angiography and Stenting) (Moscow: Geotar-Media, 2010).
4. Belenkov Yu.N., Oganov R.G. *Kardiologiya* (Cardiolog) (Moscow: Geoter-Media, 2008).
5. Blinov N.N. *Osnovy rentgenodiagnosticheskoy tekhiki* (Fundamentals of X-ray Diagnostic Engineering) (Moscow: Meditsina, 2002).
6. Artyukov I.A., Dyachkov N.V., Feshchenko R.M., Polunina A.V., Popov N.L., Shvedunov V.I., Vinogradov A.V. *Proc. SPIE*, **10243**, 1024307-1 (2017).
7. Anderson S.G., Barty C.P.J., Betts S.M., Brown W.J., Crane J.K., et al. *Appl. Phys. B*, **78** (7–8), 891 (2004).
8. Bessonov E.G., Gorbunkov M.V., Kostryukov P.V., Maslova Yu.Ya., Tunkin V.G., Postnov A.A., Mikhailichenko A.A., Shvedunov V.I., Ishkhanov B.S., Vinogradov A.V. *J. Instrum.*, **4** (7), P07017 (2009).
9. Shimuzu H., Akemoto M., Arai Y., Araki S., Aryshev A., Fukuda M., et al. *Nucl. Instrum. Methods Phys. Res. Sect. A: Accel. Spectrom. Detect. Assoc. Equip.*, **772**, 26 (2015).
10. Eggl E., Dierolf M., Achterhold K., Jud C., Gunther B., Braig E., Gleich B., Pfeiffer F. *J. Synchrotron Radiat.*, **23** (5), 1137 (2016).
11. Vaccarezza C. et al. DOI information: 10.1016/j.nima.2016.01.089.
12. Zomer F. et al. https://agenda.infn.it/conferenceDisplay.py?confId= 11130.
13. Rubenstein E., Hofstadter R., Zeman H.D., Thompson A.C., Otis J.N., Brown G.S., Giacomini J.C., Gordon H.J., Kernoff R.S., Harrison D.C. *Proc. Natl. Acad. Sci. USA*, **83** (24), 9724 (1986).
14. Dix W.-R., Engelke K., Glüer C.-C., Graeff W., Höppner C.P., Stellmaschek K.-H., Wroblewski T., Bleifeld W., Höhne K.H., Kupper W. *Nucl. Instrum. Methods Phys. Res. A*, **246** (1–3), 702 (1986).
15. Dementyev E.N., Dovga E.Ya., Kulipanov G.N., Medvedko A.S., Mezentsev N.A., Pindyurin V.F., Sheromov M.A., Skrinsky A.N., Sokolov A.S., Ushakov V.A., Zagorodnikov E.I., Kaidorin A.G., Neugodov Yu.V. *Nucl. Instrum. Methods Phys. Res. A*, **246** (1–3), 726 (1986).
16. Akisada M., Ando M., Hyodo K., Hasegawa S., Konishi K., Nishimura K., Maruhashi A., Toyofuku F., Suwa A., Kohra K. *Nucl. Instrum. Methods Phys. Res. A*, **246** (1–3), 713 (1986).
17. Pelka J.B. *Acta Phys. Polon. A*, **2** (114), 309 (2008).
18. Umetani K., Fukushima K. *Rev. Sci. Instrum.*, **84** (3), 034302 (2013).
19. Gislason-Lee A., Hoornaert B., Cowen A.R., Davies A.G. http://eprints.whiterose.ac.uk/78474/.
20. Dyachkov N.V., Polunina A.V., Popov N.L., Vinogradov S.L., Vinogradov A.V. *Biomed. Phys. Eng. Express*, **3** (5), 057001 (2017).
21. Blinov N.N., Varshavskii Yu.V., Zelikman M.I., Kondrashin S.A., Kruchinin S.A., Ternovoi S.K. *Radiologiya i Praktika*, **3**, 30 (2009).
22. Bouzarjomehri F., Tsapaki V. *Iran. J. Radiat. Res.*, **6** (4), 167 (2009).
23. Stratis A.I., Anthopoulo P.L., Gavaliatsis I.P., Ifantis G.P., Salahas A.I., Antonellis I.P., Tavernarakis A.G., Molfetas M.I. *Hellenic J.Cardiol.*, **50**, 17 (2009).
24. Pantos I., Patatoukas G., Katritsis D.G., Efstathopoulos E. *Curr. Cardiol. Rev.*, **5** (1), 1 (2009).
25. Tsapaki V. *Imaging Med.*, **2** (3), 303 (2010).
26. Miller D.L., Hilohi C.M., Spelic D.C. *Med. Phys.*, **39** (10), 6276 (2012).
27. Conti C.R. *Europ. Heart J.*, **35**, 599 (2014).
28. Olcay A., Guler E., Karaca I.O., Omaygenc M.O., Kizilirmak F., Olgun E., Yenipinar E., Cakmak H.A., Duman D. *J. Invasive Cardiol.*, **27** (4), 199 (2015).
29. Harbron R.W., Dreuil S., Bernier M.O., Pearce M.S., Thierry-Chef I., Chapple C.L., Baysson H. *J. Radiol Prot.*, **36** (4), R131 (2016).
30. Gkanatsios N.A., Huda W., Peters K.R. *Medical Phys.*, **29** (8), 1643 (2002).
31. Kulikov O.F. *Trudy FIAN*, **80**, 3 (1975).
32. Carroll F.E., Waters J.W., Price R.R., Brau C.A., Roos C.F., Tolk N.H., Pickens D.R., Stephens W.H. *Investigat. Radiol.*, **25** (5), 465 (1990); Carroll F.E. *Am. J. Roentgenol.*, **179** (3), 583 (2002).
33. http://lynceantech.com/.
34. Zhijun Chi, Yingchao Du, Lixin Yan, Zheng Zhou, Zhen Zhang, Dong Wang, Qili Tian, Hongze Zhang, Jianfei Hua, Jiaru Shi, Wenhui Huang, Huaibi Chen, Chuanxiang Tang. *Proc. SPIE*, **10391**, 103910Z-1 (2017).
35. Alesini D. DOI:http://dx.doi.org/10.23730/CYRSP-2018-001.79.
36. Landau L.D., Lifshits E.M. *The Classical Theory of Fields* (Pxford: Butterworth-Heinemann, 1987; Moscow: Nauka, 1988).
37. Batygin V.V., Toptygin I.N. *Sbornik zadach po elektrodinamike* (Collection of Problems in Electrodynamics) (Moscow: R&C Dynamics, 2002).
38. Brown W.J., Hartemann F.V. *AIP Conf. Proc.*, **737**, 839 (2004).
39. Artyukov I.A., Bessonov E.G., Gorbunkov M.V., Maslova Yu.Ya., Popov N.L., Vinogradov A.V. *Las. Part. Beams*, **34** (4), 637 (2016).

40. Deitrick K., Delayen J.R., Krafft G.A. *Proc. IPAC* (Copenhagen, Denmark, 2017) p. 932.
41. Marsh R.A., Gibson D.J. *Proc. IPAC* (Copenhagen, Denmark, 2017) p. 795.
42. Tajima H.T., Anderson G.G., Gibson D.J., Marsh R.A., Barty C.P.J. *Proc. IPAC* (Copenhagen, Denmark, 2017) p. 3656.
43. Breitkopf S., Eidam T., Klenke A., Carstens H., Holzberger S., Fill E., Schreiber T., Krausz F., Tünnermann A., Pupeza I., Limpert J. *Europ. Phys. J. Special Topics*, **224** (13), 2573 (2015).
44. Bessonov E.G., Gorbunkov M.V., Maslova Yu.Ya., Kostryukov P.V., Tunkin V.G., Ishkhanov B.S., Shvedunov V.I., Vinogradov A.V. *Proc. SPIE*, **6702**, 67020E-1 (2007).
45. Bessonov E.G., Gorbunkov M.V., Ishkhanov B.S., Kostryukov P.V., Maslova Yu.Ya., Shvedunov V.I., Tunkin V.G., Vinogradov A.V. *Laser Part. Beams*, **26** (3), 489 (2008).
46. Palmer D.T. PhD Thesis (Stanford Univ., California, 1998).
47. Hong J., Han J.-H., Park S.J., Jung Y.G., Kim D.E., Kang H.-S., Pflueger J. *High Power Laser Sci. Eng*., **3**, e21 (2015); doi:10.1017/hpl.2015.18.
48. Limpert J., Tünnermann A., Weitenberg J., Yost D.C., Al-Ghamdi A., Alahmed Z., Azzeer A., Apolonski A., Fill E., Krausz F., Pupeza I. *Opt. Lett*., **39** (9), 2595 (2014).
49. Yu H., Zhang P., Wang X., Zhou P., Chen J. *IEEE Photon. J*., **8** (2), 1 (2016).
50. Carr R. *Nucl. Instrum. Meth. Phys. Res. A*, **347** (1–3), 510 (1994).
51. Nakajima K., Nakanishi H., Ogata A., Zhang F.Q., Kumada M. *Proc. PAC*, **97**, 2371 (1997).
52. Bessonov E.G., Vinogradov A.V., Gorbunkov M.V., Turyanskii A.G., Feshchenko R.M., Shabalin Yu.V. *Phys. Usp*., **46** (8) 872 (2003) [*Usp. Fiz. Nauk*, **173** (8), 899 (2003)].
53. Gorbunkov M.V., Tunkin V.G., Bessonov E.G., Fechtchenko R.M., Artyukov I.A., Shabalin Yu.V., Kostryukov P.V., Maslova Yu.Ya., Poseryaev A.V., Shvedunov V.I., Vinogradov A.V., Mikhailchenko A.A., Ishkhanov B.S. *Soft X-ray Las. Applicat. VI, SPIE*, **5919**, 59190U (2005).
54. Vinogradov A.V., Vinogradov S.L., D'yachkov N.V., Postnov A.A., Polunina A.V. *Quantum Electron*., **47** (1), 75 (2017) [*Kvantovaya Elektron*., **47** (1), 75 (2017)].
55. Sprangle P., Ting A., Esarey E., Fisher A. *J. Appl. Phys*., **72** (11), 5032 (1992).
56. Bessonov E.G., Gorbunkov M.V., Maslova Y.Y., Kostryukov P.V., Tunkin V.G., Ishkhanov B.S., Shvedunov V.I., Vinogradov A.V. *Proc. SPIE*, **6702**, 67020E (2007).
57. Jovanovic I., Shverdin M., Gibson D., Brown C. *Nucl. Instrum. Methods Phys. Res. Sect. A: Accel. Spectrom. Detect. Assoc. Equip*., **578** (1), 160 (2007).
58. US Patent WO 2006104956 A9 (Jan 11, 2007).
59. Maslova Yu.Ya. Kand. Diss. (Moscow: Lebedev Physical Institute of RAS, 2015).
60. Artyukov I.A., Vinogradov A.V., Feshchenko R.M. *Fizicheskiye Osnovy Priborostroyeniya*, **5** (3), 56 (2016).
61. Polyakov S.N., Artuykov I.A., Blank V.D., Zholudev S.I., Feshchenko R.M., Popov N.L., Yaroslavtsev A.A., Vinogradov A.V. *X-ray Las. Coh. X-ray Sources: Development Applicat. Intern. Soc. Opt. Photon*., **10243**, 102430Y (2017).